Tunneling anisotropic magnetoresistance in fully epitaxial magnetic tunnel junctions with different barriers

B S Tao, L N Jiang, W J Kong, W Z Chen, Bin Yang, X. Wang, C. Wan, H. Wei, M. Hehn, D. Lacour, et al.

Tunneling anisotropic magnetoresistance in fully epitaxial magnetic tunnel junctions with different barriers

B. S. Tao, L. N. Jiang, W. J. Kong, W. Z. Chen, B. S. Yang, X. Wang, C. H. Wan, H. X. Wei, M. Hehn, D. Lacour, Y. Lu, and X. F. Han

Citation: Appl. Phys. Lett. **112**, 242404 (2018); doi: 10.1063/1.5027909
View online: https://doi.org/10.1063/1.5027909
View Table of Contents: http://aip.scitation.org/toc/apl/112/24
Published by the American Institute of Physics

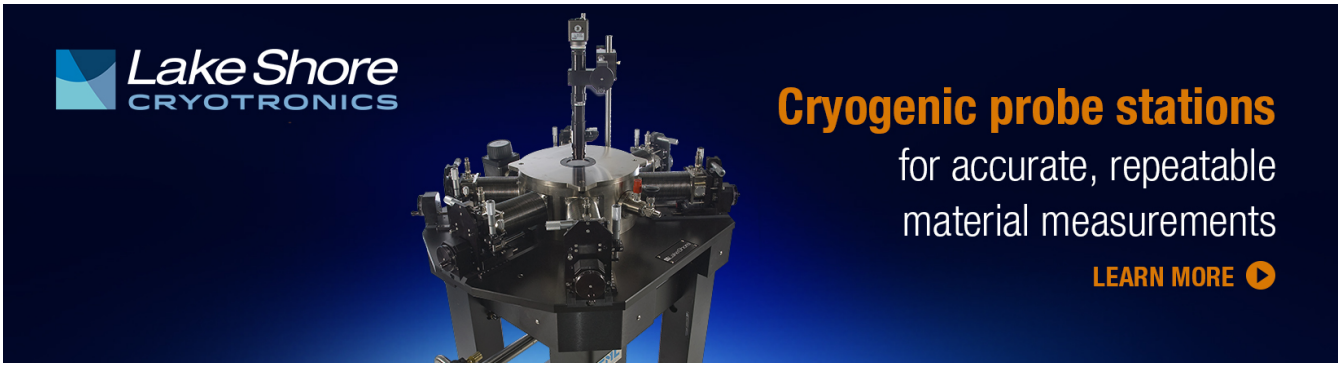

Tunneling anisotropic magnetoresistance in fully epitaxial magnetic tunnel junctions with different barriers

B. S. Tao,[1,2,3] L. N. Jiang,[2] W. J. Kong,[2] W. Z. Chen,[2] B. S. Yang,[2] X. Wang,[2] C. H. Wan,[2] H. X. Wei,[2] M. Hehn,[3] D. Lacour,[3] Y. Lu,[3,a)] and X. F. Han[2,a)]
[1]*Institute of Electrical Engineering, Chinese Academy of Sciences, Beijing 100190, China*
[2]*Beijing National Laboratory of Condensed Matter Physics, Institute of Physics, University of Chinese Academy of Sciences, Chinese Academy of Sciences, Beijing 100190, China*
[3]*Institut Jean Lamour, UMR 7198, CNRS-Université de Lorraine, BP239, 54506 Vandoeuvre-lès-Nancy, France*

(Received 7 March 2018; accepted 27 May 2018; published online 12 June 2018)

We report the tunneling anisotropic magnetoresistance (TAMR) in fully epitaxial Fe/*Barrier*/Fe (001) magnetic tunnel junctions (MTJs) where the *Barrier* is annealed MgO, $MgAlO_x$, MgO-$MgAlO_x$, or as-grown MgO/$MgAlO_x$. The TAMR was measured as the magnetization of Fe electrodes rotated from in-plane to out-of-plane. The angular dependence of TAMR for all samples exhibited superposed behavior of twofold and fourfold symmetries. The proportion of fourfold symmetry is larger in MTJs with MgO and MgO-$MgAlO_x$ than that in MTJs with $MgAlO_x$ and MgO/$MgAlO_x$ barriers. By characterizing inelastic electron tunneling spectroscopy in the antiparallel state and parallel conductance of the MTJs, we revealed diverse minority interfacial resonant states (IRSs) and different contributions from Δ_1 and Δ_5 symmetry states to the conductance in the MTJs. Our results illustrate that the minority IRS dominated by Δ_5 symmetry can mix with majority Δ_1 states and give rise to the enhanced fourfold symmetric angular dependence in MTJs with MgO and MgO-$MgAlO_x$ barriers. *Published by AIP Publishing.* https://doi.org/10.1063/1.5027909

Tunneling magnetoresistance (TMR) in magnetic tunnel junctions (MTJs) has been extensively studied[1–5] due to its important applications in spintronic devices. The TMR originates from spin-dependent tunneling between two ferromagnetic electrodes through a thin barrier. Different from TMR, tunneling anisotropic magnetoresistance (TAMR), which is caused by the interplay between anisotropic density of states (DOS) of magnet and magnetization, requires only one magnetic electrode in the junctions.[6,7] The simplicity of the structures for TAMR is attractive for applications and has attracted much attention.[6,8–14] The anisotropy of DOS with respect to the magnetization direction is attributed to spin-orbit coupling (SOC).[9,10] Relatively large TAMR was observed in junctions consisting of materials with strong SOC, such as GaMnAs[8,15] and Pt.[13] Furthermore, a finite TAMR was also noticed in MTJs with transition metal[11–13,16] despite the weak SOC in the system.

The TAMR in AlO_x or MgO barrier based MTJs has been experimentally reported,[11,13,16,17] and the angular dependence with twofold and fourfold components was observed, which is attributed to minority interfacial resonant states (IRSs) coupled to Δ_1 states.[11] In epitaxial Fe/MgO/Fe MTJ, different minority IRSs have been revealed[17,18] and a relatively large TAMR was observed[17] due to the shift of the resonant surface band via the Rashba effect.[10] It seems that the minority IRSs have a significant impact on TAMR. Recently, the $MgAlO_x$ oxide with the spinel structure has been investigated as a promising candidate for the MTJ barrier due to its smaller lattice mismatch with a usual ferromagnetic electrode.[19–24] An improved bias dependence of TMR[19,25] and enhanced quantum well states[26] in $MgAlO_x$ barrier based MTJs have been realized owing to the high quality of the $MgAlO_x$/ferromagnet interfaces. The IRSs, which impact the TAMR effect, should be modified in MTJs with different barriers. In this work, we studied the TAMR and its angular dependence in fully epitaxial MTJs with four kinds of barriers (annealed MgO, $MgAlO_x$, MgO-$MgAlO_x$, or as-grown MgO/$MgAlO_x$ barrier), where different IRSs were observed by inelastic electron tunneling spectroscopy (IETS) in the different samples. The TAMR displayed different symmetries of angular dependence, and its relationship with IRSs has been discussed.

MTJs with different barriers were grown on MgO substrates by molecular beam epitaxy (MBE) with the following structure: Fe(45 nm)/*Barrier*/Fe(10 nm)/Co(20 nm)/Au(15 nm). Before depositing the multilayers, the MgO substrate was first annealed at 650 °C for 30 min and 10 nm MgO seed layer was deposited. The bottom Fe of all the samples was annealed *in situ* at 500 °C for 30 min to flatten the surface. Then, the *Barrier* layers were deposited at room temperature (RT). The thickness is controlled by the intensity oscillation of reflective high energy electron diffraction (RHEED) with monolayer (ML) precision. Three samples were prepared with the *Barrier* of MgO (12 ML), $MgAlO_x$(12 ML), or MgO(5 ML)/$MgAlO_x$(7 ML). The top Fe of the three samples was annealed at 400 °C to improve the quality of crystallinity. Hereafter, they are named as MgO, $MgAlO_x$, and MgO-$MgAlO_x$ MTJ, respectively. For comparison, another sample with a MgO(5 ML)/$MgAlO_x$(7 ML) barrier but the top Fe without any annealing was deposited to avoid the mixture of MgO and $MgAlO_x$ during annealing,[25] hereafter, named as MgO/$MgAlO_x$ MTJ. All the samples were patterned into junctions with a size of $20 \times 20\ \mu m^2$ by UV lithography combined with ion milling. The transport properties were

a)Authors to whom correspondence should be addressed: yuan.lu@univ-lorraine.fr and xfhan@iphy.ac.cn

measured by the two-probe method, where negative bias corresponds to the electrons tunneling from the top to bottom electrode. The TAMR measurement was performed at 10 K in a Physical Property Measurement System (PPMS) by measuring the differential resistance $R_d = dV/dI$ using an AC lock-in method. The magnetic easy axis of the electrode, the film normal direction $\vec{n}$, and the magnetic field $\vec{H}$ were arranged in the same plane. The schematics of the measurement setup and structure of MTJs are shown in Fig. 1(a). R_d was measured as a function of angle θ between $\vec{H}$ and $\vec{n}$, where a magnetic field of 5 T was applied to saturate the magnetization of electrodes and the sample was rotated from $\theta = 0°$ to $\theta = 360°$.

Figure 1(b) shows the temperature dependence of the TMR ratio of all the samples at a bias voltage of 10 mV. A common feature is that the TMR ratio increases with the decreasing temperature, resulting from that R_{AP} increases rapidly while R_P varies slightly with decreasing temperature. As shown in Fig. 1(b), we can obtain a TMR ratio of 154% at room temperature (RT) and 305% at 20 K for MgO MTJ, indicating the high quality of MgO MTJ. A much lower TMR ratio at RT (74%) and 20 K (121%) was gained for $MgAlO_x$ MTJ. This could be explained by the "band folding" effect of Fe in the $MgAlO_x$ barrier,[21] which creates a new conductive channel in the minority states with Δ_1 symmetry and reduces the effective spin-polarization of the Fe

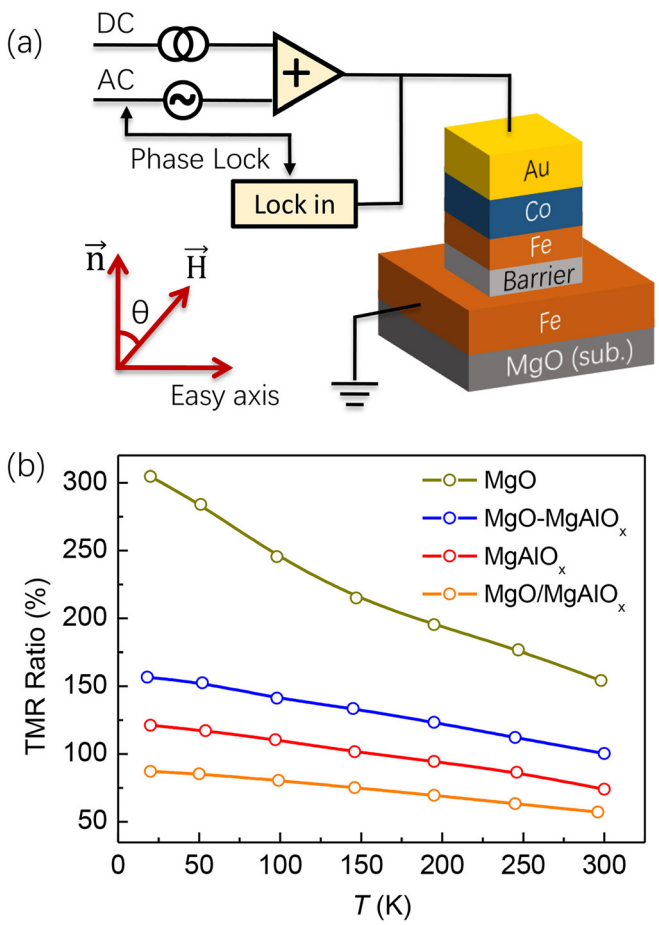

FIG. 1. (a) Schematics of the MTJ structure and measurement setup for TAMR by an AC lock in method and (b) temperature dependence of the TMR ratio of MgO, $MgAlO_x$, MgO-$MgAlO_x$, and MgO/$MgAlO_x$ MTJs at a bias of 10 mV.

electrode. The TMR ratio is improved in the composite MgO-$MgAlO_x$ MTJ, which is 100% at RT and 157% at 20 K, indicating a suppression of the "band folding" effect. While for MgO/$MgAlO_x$ MTJ with un-annealed top Fe, the TMR is only 57% at RT and 87% at 20 K, which is even lower than that of $MgAlO_x$ MTJ. This result demonstrates that the annealing process is necessary to improve the TMR in fully epitaxial MTJs.[27]

The angular dependence of R_d with bias voltage from −0.9 V to 0.9 V is shown in Figs. 2(a)–2(d) for MgO, $MgAlO_x$, MgO-$MgAlO_x$, and MgO/$MgAlO_x$ MTJs, respectively, where ϕ denotes the angle between the Fe magnetization direction and film normal $\vec{n}$. R_d is normalized to its average value over θ at each bias. After taking into account the Zeeman and the demagnetization energy, the relation between θ and ϕ can be given by minimizing the total energy

$$HM_s \sin(\phi - \theta) - 2\pi M_s^2 \sin 2\phi = 0\,, \tag{1}$$

where H is the magnetic field and M_s is the saturation magnetization of Fe. The red solid curves are fitting results by the following equation:

$$R_d = A_0 + A_2 \cos 2\phi + A_4 \cos 4\phi\,, \tag{2}$$

where A_0, A_2, and A_4 are the fitting parameters. Taking $4\pi M_s = 2.1$ T,[28] we can obtain very good agreement between data and fits.

For MgO and MgO-$MgAlO_x$ MTJs, the angular dependence shows pronounced components of twofold and

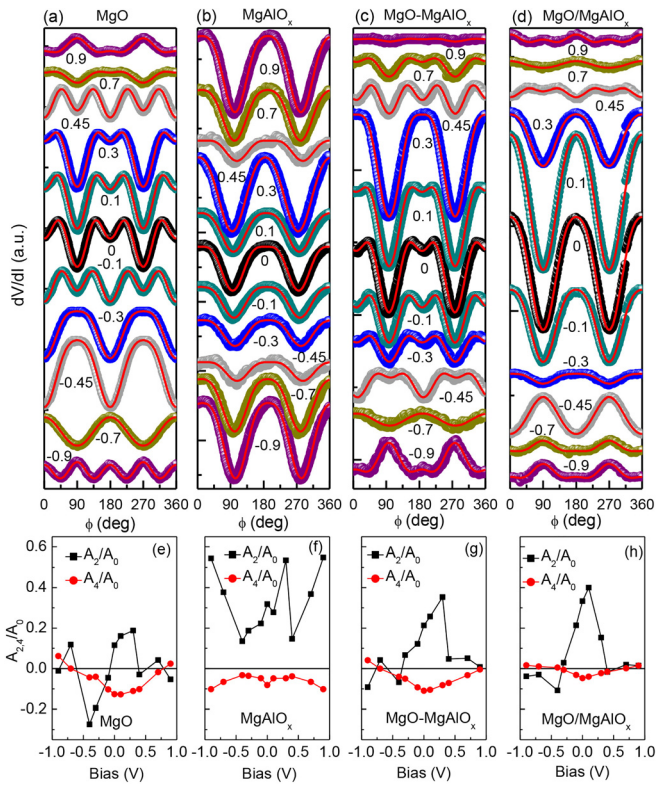

FIG. 2. Normalized dV/dI as a function of ϕ at different bias for MgO (a), $MgAlO_x$ (b), MgO-$MgAlO_x$ (c), and MgO/$MgAlO_x$ (d), respectively, where symbols are experimental data and the red lines are fitting curves. The numbers in the figure denote the value of bias voltage. There is a vertical offset between different curves for clarity. (e) and (f) show the corresponding fitting parameters A_2/A_0 (black) and A_4/A_0 (red) dependence on bias.

fourfold symmetries and the position of the R_d extrema changes at different bias. For $MgAlO_x$ MTJ, the TAMR curves are mainly dominated by twofold symmetry and the minimum of R_d is observed at $\phi = 90°$ and 270° for all bias voltages, which is quite different from that of MgO MTJ. The angular dependence of MgO/$MgAlO_x$ MTJ is also dominated by the twofold component, but its extrema vary with bias. To estimate the proportion of twofold and fourfold components of angular dependence of R_d, we plotted A_2/A_0 and A_4/A_0 as a function of bias as shown in Figs. 2(e)–2(h). For $MgAlO_x$ MTJ, the TAMR effect is much increased and the sign of A_2 and A_4 exhibits no change with bias. The proportion of twofold symmetry is much higher than that of fourfold symmetry. Generally, the angular dependence of the TAMR effect in MTJs is twofold-symmetrical.[11,29] Thus, the enhancement of the TAMR effect in $MgAlO_x$ MTJ is mainly presented by A_2/A_0 and no much increase was observed in A_4/A_0. While for the other three samples, A_2 and A_4 change their sign with bias and A_4 shows a parabolic like behavior as a function of bias. In addition, MgO/$MgAlO_x$ MTJ shows a much weaker fourfold component than MgO and MgO-$MgAlO_x$ MTJs.

To give a comprehensive perspective of the TAMR, Figs. 3(a)–3(d) show the normalized R_d as a function of bias voltage and angle θ with steps of 50 mV and 2°, respectively. The magnitude of R_d is represented by the color in the plot. Noticeably, $MgAlO_x$ MTJ shows distinct features from the other three samples. The angular dependence of $MgAlO_x$ MTJ mainly shows a twofold symmetry, and the bias dependence is rather symmetric about zero bias. The minima of R_d are at $\theta = 90°$ and 270° for all bias voltage from −1.2 V to 1.2 V, and the amplitude of TAMR increases with increasing bias voltage. While, for the other three samples, the bias and angle dependence of R_d are rather complicated compared to those reported in CoFe-MgO-CoFe MTJs,[11] we can still extract some common features for the three samples. First, their bias dependence is asymmetric and the TAMR is large at low bias. Second, within the bias range around from −0.3 V to 0.3 V, the minimum of R_d is at $\theta = 90°$ and 270°, while for bias voltage below −0.3 V, the maximum of R_d locates at $\theta = 90°$ and 270°, indicating a sign change of TAMR. With further decreasing bias voltage, there is a sign change again in MgO and MgO-$MgAlO_x$ MTJs but the MgO/$MgAlO_x$ MTJ remains the same. For bias below −0.8 V, there is a clear second set of peaks in MgO and MgO-$MgAlO_x$ MTJs, indicating a clear evidence of fourfold symmetric angular dependence, but no obvious change was observed in MgO/$MgAlO_x$ MTJs.

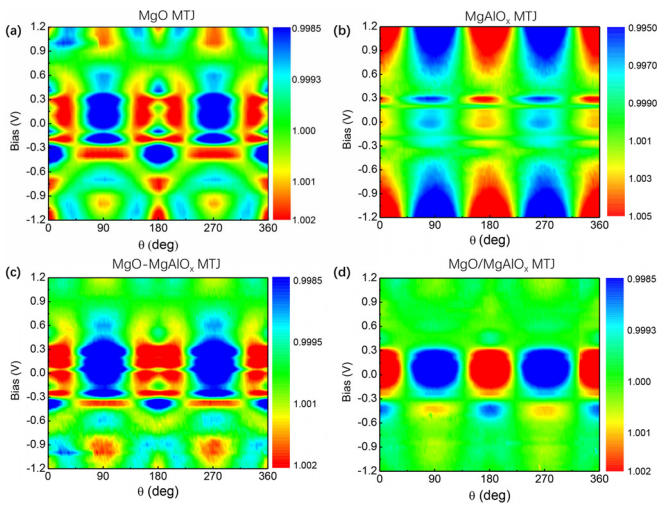

FIG. 3. Normalized dV/dI as a function of bias voltage and angle θ for MgO (a), $MgAlO_x$ (b), MgO-$MgAlO_x$ (c), and MgO/$MgAlO_x$ (d) MTJs, respectively. The magnitude of dV/dI is shown by the color.

It is well known that the minority IRSs related to interfacial electronic structures also have an important impact on transport properties,[18,30,31] which possibly accounts for the observed different TAMR behavior in MTJs with different barriers. To identify the minority IRSs, we performed the IETS measurement of the samples in the antiparallel (AP) state. It is easy to clarify the minority IRSs in the AP state when electrons tunnel from occupied majority states to unoccupied minority states. Figures 4(a)–4(d) show d^2I/dV^2 curves in the AP state at different temperatures for MgO, $MgAlO_x$, MgO-$MgAlO_x$, and MgO/$MgAlO_x$ MTJs, respectively. The insets are corresponding zoom-in of the area in the dashed square. For MgO MTJ, there are several clear peaks, which is consistent with the reported results.[17] The peaks at ±0.03 V can be attributed to magnon excitation[32] related to the spin-flip events in the AP state. The peaks at −0.16 V and −1.0 V labeled as IRS1 and IRS2, respectively, are attributed to IRS at the bottom Fe/MgO interface. It has been well established that both IRSs contain minority Δ_1 states and minority Δ_5 states, but IRS1 is dominated by minority Δ_5 states, while IRS2 is dominated by minority Δ_1 states.[17] The IRSs are very sensitive to chemical bonding [17]and roughness or defects at the interface.[18] No peaks were observed at positive bias, indicating that the IRSs vanished at the top MgO/Fe interface due to the roughness of the top interface. For $MgAlO_x$ MTJ, no IRSs but only weak magnon peaks were observed. The disappearance of IRSs at the Fe/$MgAlO_x$ interface is reasonable due to different electronic structures and interfacial environments. The lattice constant of the spinel $MgAl_2O_4$ barrier is twice that of the Fe electrode, resulting in the "band-folding" effect in Fe,[21] which leads to different interfacial band structures. In addition, the stable Fe/$MgAl_2O_4$ interface is Fe atoms on top of O atoms of $MgAl_2O_4$ with octahedral Al terminated,[21] which is different from that of MgO MTJ.

For the MgO-$MgAlO_x$ sample, the d^2I/dV^2 curve shows the same peaks of magnon, IRS1, and IRS2 as that of MgO MTJs. This proves that the Fe/MgO-$MgAlO_x$ interface is the same as that of MgO MTJ and there is no Al diffusion into the interface during the annealing process. However, for MgO/$MgAlO_x$ MTJ, there are only peaks of magnon and IRS1 in the d^2I/dV^2 curve. This proves that the annealing process not only improves the crystal quality of the top Fe electrode but also modifies the bottom Fe/MgO interface environment. The bottom Fe electrodes of MgO-$MgAlO_x$ and MgO/$MgAlO_x$ MTJs were annealed *in situ* to flatten the surface, and the barriers were grown in a two-dimensional layer-by-layer mode. The roughness of the bottom interfaces and crystal ordering of barriers should be the same for the two samples, which change slightly during annealing of the top Fe film in MgO-$MgAlO_x$ MTJ. The difference of

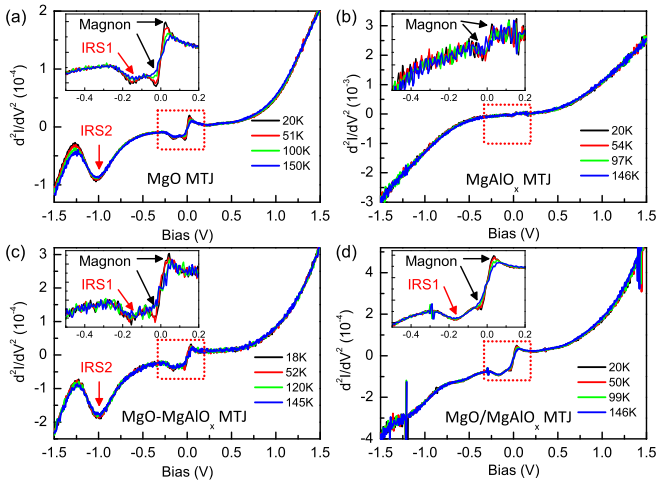

FIG. 4. Inelastic electron tunneling spectroscopy (IETS) in AP states at different temperatures for MgO (a), MgAlO$_x$ (b), MgO-MgAlO$_x$ (c), and MgO/MgAlO$_x$ (d) MTJs, respectively. Insets show the zoom-in of the area in the dashed square. Magnon peaks and IRSs are denoted.

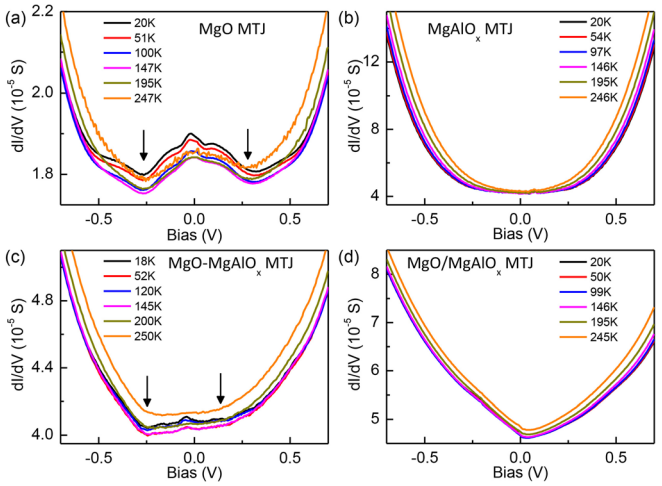

FIG. 5. Parallel differential conductance at different temperatures for MgO (a), MgAlO$_x$ (b), MgO-MgAlO$_x$ (c), and MgO/MgAlO$_x$ (d) MTJs, respectively. The arrows in (a) and (c) denote the local minima of the conductance.

interfaces for the two samples may be attributed to Fe oxide. In typical epitaxial Fe/MgO/Fe MTJ, the existence of FeO oxide at the bottom interface has been proposed.[33] The Fe oxide at the un-annealed Fe/MgO bottom interface may be different. It has been proved that the annealing process can transform the interfacial oxide from a more Fe_2O_3-like phase in the as-grown state to a more FeO-like phase.[34] The modification of Fe oxide at the interface can account for the different IRSs in the MgO-MgAlO$_x$ and MgO/MgAlO$_x$ MTJs.

The role of IRS in transport can be evidenced by characterization of parallel conductance of MTJ. Figures 5(a)–5(d) show the parallel differential conductance at different temperatures for MgO, MgAlO$_x$, MgO-MgAlO$_x$, and MgO/MgAlO$_x$ MTJs, respectively. The conductance of MgO MTJ shows a bump between ± 0.25 V, which is a typical feature of single crystal MgO MTJ.[35] The bump reflects the majority Δ_5 band structure of bulk Fe (001), which lies at about 0.2 eV above the Fermi level. When the bias voltage is larger than 0.2 V, the contribution from Δ_5 states to the conductance is eliminated, resulting in a local minimum of the conductance. The conductance of MgAlO$_x$ MTJ is quite flat between ± 0.25 V. This indicates a negligible contribution from the Δ_5 band compared with the Δ_1 band due to large contribution of Δ_1 states in both majority and minority channels in P states.[21] The MgO-MgAlO$_x$ MTJ shows a similar characteristic to that of MgO MTJ, while we could not find any local minima in the conductance spectrum of the MgO/MgAlO$_x$ MTJ.

We argue that the different electronic structures are responsible for the different TAMR behaviors of the MTJs. The main difference of the TAMR is the symmetry of angular dependence, i.e., the proportion of fourfold symmetry in MgO and MgO-MgAlO$_x$ MTJs is much higher than that in MgAlO$_x$ and MgO/MgAlO$_x$ MTJs. The angular dependence of out-of-plane TAMR is twofold-symmetrical only if the second order of the SOC field is considered.[29] The fourfold component of TAMR was also observed in sputtered MgO MTJ and attributed to the coupling of minority IRS and majority Δ_1 band.[11] Furthermore, it has been confirmed that the IRS1 dominated by minority Δ_5 states can mix with majority Δ_1 states via SOC at the interface to generate new states in single crystal Fe/MgO/Fe MTJ.[17] The new states contribute to the Δ_5 related conductance bump mentioned above and result in an nonmonotonic temperature dependence of conductance at low bias.[17] In our case, the parallel conductance within bump range shows nonmonotonic temperature dependence and minimum locates at around $T = 150$ K, as shown in Figs. 5(a) and 5(c), which is consistent with the reported results.[17] Therefore, we argue that the mixture of IRS1 and majority Δ_1 states gives rise to the enhanced fourfold symmetric angular dependence of TAMR in MgO and MgO-MgAlO$_x$ MTJs. The mixture state is not only a mixture of Δ_1 and Δ_5 symmetry but also the mixture of spin-up and spin-down, which can contribute to the parallel conductance with both negative bias and positive bias, resulting in the related local minimum of parallel conductance. Thus, A_4/A_0 is symmetric as a function of voltage though the IRS can only be detected in negative bias. For MgO/MgAlO$_x$ MTJ, the IRS1 cannot mix with majority Δ_1 states efficiently, which can be confirmed by the featureless parallel conductance. Thus, MgO/MgAlO$_x$ MTJ shows a much weaker fourfold symmetric angular dependence of TAMR. For the same reason, MgAlO$_x$ MTJ without of IRSs shows a main twofold symmetric angular dependence of TAMR.

In summary, we fabricated four different fully epitaxial MTJs with the core structure of Fe/*Barrier*/Fe (001), where the *Barrier* is MgO, MgAlO$_x$, MgO-MgAlO$_x$, and MgO/MgAlO$_x$, respectively. All the Fe layers were *in situ* annealed to improve the crystal quality and flatten the surface except the top Fe layer of MgO/MgAlO$_x$ MTJ. The highest TMR ratio is obtained in MgO MTJ, while MgO/MgAlO$_x$ MTJ shows the lowest TMR. The TAMR effect in these MTJs was characterized at 10 K with the magnetization of Fe tilted from in-plane to out-of-plane at different bias voltages. The angular dependence of TAMR shows the main twofold symmetry in MgAlO$_x$ and MgO/MgAlO$_x$ MTJs, but an enhanced fourfold symmetry was observed in MgO and MgO-MgAlO$_x$ MTJs. By measuring the IETS in AP states

and parallel conductance, we found that the IRS dominated by minority Δ_5 states can mix with majority Δ_1 states in MgO and MgO-$MgAlO_x$ MTJ, giving rise to the enhanced fourfold symmetric angular dependence of TAMR.

See supplementary material for the temperature dependence of parallel and antiparallel resistance for all the samples.

This project was supported by the National Key Research and Development Program of China (Grant No. 2017YFA0206200) and the National Natural Science Foundation of China (NSFC, Grant Nos. 11434014, 51620105004, 51701203, and 11674373) and partially supported by the Strategic Priority Research Program (B) (Grant No. XDB07030200), the International Partnership Program (No. 112111KYSB20170090), and the Key Research Program of Frontier Sciences (Grant No. QYZDJ-SSW-SLH016) of the Chinese Academy of Sciences (CAS). Y.L. also acknowledges the support from the Joint French National Research Agency (ANR)-NSFC of China (NSFC) SISTER Project (Grant Nos. ANR-11-IS10-0001 and NNSFC 61161130527) and ENSEMBLE Project (Grant Nos. ANR-14-0028-01 and NNSFC 61411136001). B.S.T. also acknowledges the China Postdoctoral Science Foundation Funded Project (Grant No. 2016M601130).

[1]M. Julliere, Phys. Lett. A **54**, 225 (1975).
[2]T. Miyazaki and N. Tezuka, J. Magn. Magn. Mater. **139**, L231 (1995).
[3]J. S. Moodera, L. R. Kinder, T. M. Wong, and R. Meservey, Phys. Rev. Lett. **74**, 3273 (1995).
[4]S. S. Parkin, C. Kaiser, A. Panchula, P. M. Rice, B. Hughes, M. Samant, and S. H. Yang, Nat. Mater. **3**, 862 (2004).
[5]S. Yuasa, T. Nagahama, A. Fukushima, Y. Suzuki, and K. Ando, Nat. Mater. **3**, 868 (2004).
[6]C. Gould, C. Ruster, T. Jungwirth, E. Girgis, G. M. Schott, R. Giraud, K. Brunner, G. Schmidt, and L. W. Molenkamp, Phys. Rev. Lett. **93**, 117203 (2004).
[7]C. Fang, C. H. Wan, B. S. Yang, J. Y. Qin, B. S. Tao, H. Wu, X. Zhang, X. F. Han, A. Hoffmann, X. M. Liu, and Z. M. Jin, Phys. Rev. B **96**, 134421 (2017).
[8]C. Ruster, C. Gould, T. Jungwirth, J. Sinova, G. M. Schott, R. Giraud, K. Brunner, G. Schmidt, and L. W. Molenkamp, Phys. Rev. Lett. **94**, 027203 (2005).
[9]H. Saito, S. Yuasa, and K. Ando, Phys. Rev. Lett. **95**, 086604 (2005).
[10]A. N. Chantis, K. D. Belashchenko, E. Y. Tsymbal, and M. van Schilfgaarde, Phys. Rev. Lett. **98**, 046601 (2007).
[11]L. Gao, X. Jiang, S. H. Yang, J. D. Burton, E. Y. Tsymbal, and S. S. Parkin, Phys. Rev. Lett. **99**, 226602 (2007).
[12]J. Moser, A. Matos-Abiague, D. Schuh, W. Wegscheider, J. Fabian, and D. Weiss, Phys. Rev. Lett. **99**, 056601 (2007).
[13]B. G. Park, J. Wunderlich, D. A. Williams, S. J. Joo, K. Y. Jung, K. H. Shin, K. Olejnik, A. B. Shick, and T. Jungwirth, Phys. Rev. Lett. **100**, 087204 (2008).
[14]X. Z. Chen, J. F. Feng, Z. C. Wang, J. Zhang, X. Y. Zhong, C. Song, L. Jin, B. Zhang, F. Li, M. Jiang, Y. Z. Tan, X. J. Zhou, G. Y. Shi, X. F. Zhou, X. D. Han, S. C. Mao, Y. H. Chen, X. F. Han, and F. Pan, Nat. Commun. **8**, 449 (2017).
[15]A. D. Giddings, M. N. Khalid, T. Jungwirth, J. Wunderlich, S. Yasin, R. P. Campion, K. W. Edmonds, J. Sinova, K. Ito, K. Y. Wang, D. Williams, B. L. Gallagher, and C. T. Foxon, Phys. Rev. Lett. **94**, 127202 (2005).
[16]S. Hatanaka, S. Miwa, K. Matsuda, K. Nawaoka, K. Tanaka, H. Morishita, M. Goto, N. Mizuochi, T. Shinjo, and Y. Suzuki, Appl. Phys. Lett. **107**, 082407 (2015).
[17]Y. Lu, H. X. Yang, C. Tiusan, M. Hehn, M. Chshiev, A. Duluard, B. Kierren, G. Lengaigne, D. Lacour, C. Bellouard, and F. Montaigne, Phys. Rev. B **86**, 184420 (2012).
[18]P. J. Zermatten, G. Gaudin, G. Maris, M. Miron, A. Schuhl, C. Tiusan, F. Greullet, and M. Hehn, Phys. Rev. B **78**, 033301 (2008).
[19]H. Sukegawa, H. Xiu, T. Ohkubo, T. Furubayashi, T. Niizeki, W. Wang, S. Kasai, S. Mitani, K. Inomata, and K. Hono, Appl. Phys. Lett. **96**, 212505 (2010).
[20]J. Zhang, X. G. Zhang, and X. F. Han, Appl. Phys. Lett. **100**, 222401 (2012).
[21]Y. Miura, S. Muramoto, K. Abe, and M. Shirai, Phys. Rev. B **86**, 024426 (2012).
[22]H. Sukegawa, Y. Miura, S. Muramoto, S. Mitani, T. Niizeki, T. Ohkubo, K. Abe, M. Shirai, K. Inomata, and K. Hono, Phys. Rev. B **86**, 184401 (2012).
[23]B. S. Tao, D. L. Li, H. F. Liu, H. X. Wei, J. F. Feng, S. G. Wang, and X. F. Han, IEEE Trans. Magn. **50**, 4401004 (2014).
[24]B. S. Tao, D. L. Li, Z. H. Yuan, H. F. Liu, S. S. Ali, J. F. Feng, H. X. Wei, X. F. Han, Y. Liu, Y. G. Zhao, Q. Zhang, Z. B. Guo, and X. X. Zhang, Appl. Phys. Lett. **105**, 102407 (2014).
[25]Ikhtiar, H. Sukegawa, X. Xu, M. Belmoubarik, H. Lee, S. Kasai, and K. Hono, Appl. Phys. Lett. **112**, 022408 (2018).
[26]B. S. Tao, H. X. Yang, Y. L. Zuo, X. Devaux, G. Lengaigne, M. Hehn, D. Lacour, S. Andrieu, M. Chshiev, T. Hauet, F. Montaigne, S. Mangin, X. F. Han, and Y. Lu, Phys. Rev. Lett. **115**, 157204 (2015).
[27]F. Bonell, S. Andrieu, A. M. Bataille, C. Tiusan, and G. Lengaigne, Phys. Rev. B **79**, 224405 (2009).
[28]J. Crangle and G. M. Goodman, Proc. R. Soc. London, Ser. A **321**, 477 (1971).
[29]A. Matos-Abiague, M. Gmitra, and J. Fabian, Phys. Rev. B **80**, 045312 (2009).
[30]C. Tiusan, J. Faure-Vincent, C. Bellouard, M. Hehn, E. Jouguelet, and A. Schuhl, Phys. Rev. Lett. **93**, 106602 (2004).
[31]K. D. Belashchenko, J. Velev, and E. Y. Tsymbal, Phys. Rev. B **72**, 140404(R) (2005).
[32]V. Drewello, J. Schmalhorst, A. Thomas, and G. Reiss, Phys. Rev. B **77**, 014440 (2008).
[33]S. G. Wang, G. Han, G. H. Yu, Y. Jiang, C. Wang, A. Kohn, and R. C. C. Ward, J. Magn. Magn. Mater. **310**, 1935 (2007).
[34]D. Telesca, B. Sinkovic, S.-H. Yang, and S. S. P. Parkin, J. Electron Spectrosc. Relat. Phenom. **185**, 133 (2012).
[35]C. Tiusan, F. Greullet, M. Hehn, F. Montaigne, S. Andrieu, and A. Schuhl, J. Phys.: Condens. Matter **19**, 165201 (2007).